

## **Spectral response, carrier lifetime, and photocurrents of SiC photocathodes**

Masashi Kato<sup>1\*</sup>, Keiko Miyake<sup>1</sup>, Tomonari Yasuda<sup>1</sup>, Masaya Ichimura<sup>1</sup>, Tomoaki Hatayama<sup>2</sup>, and Takeshi Ohshima<sup>3</sup>

*<sup>1</sup>Department of Engineering Physics, Electronics and Mechanics, Nagoya Institute of Technology, Nagoya 466-8555, Japan*

*<sup>2</sup>Graduate School of Materials Science, Nara Institute of Science and Technology, Ikoma, Nara 630-0192, Japan*

*<sup>3</sup>Japan Atomic Energy Agency, Takasaki, Gumma 370-1292, Japan*

\*E-mail: kato.masashi@nitech.ac.jp

Silicon carbide (SiC) photocathode is one of the candidates for energy conversion from the solar light to hydrogen gas. The conversion efficiencies using SiC photocathodes are still low for practical use. In this study, to find origins of low conversion efficiency, we evaluated carrier lifetimes and depletion layer widths in SiC photocathodes and examined relationship of them with photocurrents. In addition, we observed spectral response of the photocurrents from the photocathodes. From these results, we found that enhancement of the carrier lifetime and the depletion layer width is effective for increase of the conversion efficiency for 4H- and 6H-SiC. 3C-SiC would have defects reducing the effective carrier lifetime, and thus decrease of such defects is essential for increase of the conversion efficiency using 3C-SiC.

## 1. Introduction

The hydrogen generation using sunlight attracts attention as the next generation of energy related technologies.<sup>1-8)</sup> Among hydrogen generation techniques, the photoelectrochemical method is an environment-friendly process.<sup>7,8)</sup> However, the low conversion efficiency and corrosion of the photoelectrodes during the process are obstacles for this technology to be realizable. For example, TiO<sub>2</sub> is a conventional material for the photoelectrodes and considered highly resistive for corrosion in electrolytes, but the conversion efficiencies from solar to hydrogen energy are only 1-2%.<sup>9)</sup> This low efficiency is due to the wide band gap of TiO<sub>2</sub>, even though this material shows good spectral responses (quantum efficiencies of ~50%) at wavelengths from 300 to 400 nm.<sup>10)</sup> Meanwhile, materials other than TiO<sub>2</sub> sometimes show higher conversion efficiencies, but they are weak against corrosion.<sup>11)</sup> To overcome the corrosion problem, we have employed silicon carbide (SiC) photocathodes and have reported their durability.<sup>12-15)</sup> We have also reported that 3C-SiC is the most promising polytype for photocathodes owing to its smallest band gap (2.2 eV) among polytypes.<sup>12-15)</sup> Owing to this moderate bandgap, theoretical conversion efficiency can be > 3%, if a thickness of an absorption layer is larger than 10 μm. However, the experimental conversion efficiencies from SiC photocathodes are less than 0.4% which is not enough for practical use,<sup>15)</sup> and thus we need to identify origins of the low efficiencies for improvement.

In case of a photocathode, for reaction of ions with electrons, the photogenerated electrons must reach the electrolyte. Therefore, when the diffusion length of electrons  $L_D$  and depletion layer width  $W$  in the photocathode are large, electrons excited deep inside of the photocathode can contribute to the reaction as in solar cells, i.e., a photocathode is active for wavelengths near to that corresponding to the band gap energy, at which absorption coefficient  $\alpha$  of the material is small. Therefore, a spectral response of the photocathode depends on  $L_D$  and  $W$ . We have already briefly reported relationship of photocurrent with  $L_D$  and  $W$  for 4H- and 6H-SiC samples.<sup>16)</sup> As noted earlier, 3C-SiC is expected to show the highest conversion efficiency among SiC polytypes, but due to immature growth techniques, the control of the carrier lifetime  $\tau$  and the acceptor concentration in 3C-SiC is difficult. In this study, we analyzed effects of  $L_D$  and  $W$  on photocurrents by comparison with numerical calculations, and observed spectral response of photocurrents for 4H-, 6H- and 3C-SiC photocathodes.

## 2. Experimental methods

The samples employed in this study are listed in Table 1. “4H-bulk” is B doped bulk p-type

4H-SiC. “p4H” is an Al-doped p-type epitaxial layer grown on an 8°-off (0001) Si-face 4H-SiC substrate. p4H sample was cut into pieces and some of these were irradiated with electrons at an energy of 160 keV and doses of  $1 \times 10^{16} \text{ cm}^{-2}$  and  $1 \times 10^{17} \text{ cm}^{-2}$ .<sup>16-18)</sup> These samples were denoted as “ele16” and “ele17”, respectively. “Less  $N_A$ ” is another Al-doped p-type epitaxial layer grown on a 4°-off (0001) Si-face p-type 4H-SiC substrate. “Less  $N_A$  H<sub>2</sub>” is annealed Less  $N_A$  in H<sub>2</sub> ambient at 1000°C for  $\tau$  enhancement.<sup>19,20)</sup> “6H-bulk” is highly resistive bulk p-type 6H-SiC. “p6H” and “p3C” are Al-doped p-type epitaxial 6H- and 3C-SiC layers, respectively, which were grown on a 3.5°-off or on axis (0001) Si-face 6H-SiC substrates.

$\tau$  of these samples were measured by using the microwave photoconductivity decay ( $\mu$ -PCD) method with a 266 nm pulsed yttrium aluminum garnet (YAG) laser with a photon density of  $\sim 10^{15} \text{ cm}^{-2}$  per pulse.<sup>17)</sup> We treated 1/e lifetime as  $\tau$  in this paper, and 1/e lifetime is defined as the excess carrier decay time from a peak to 1/e. Then, photocurrents were measured in three and two electrode systems. For the three electrode system, Pt electrode and saturated calomel electrode (SCE) were used as counter and reference electrodes, respectively. The sample was placed on a plastic plate by wax and the surface was exposed. An ohmic contact on the samples was connected to a potentiostat and the applied potential was controlled to 0 V vs SCE. Figure 1(a) shows schematic of the placed sample. In the two electrode system, no reference electrode was used and Ni or Al was utilized as counter electrode. In both systems, the electrolyte contained 1 mol/L H<sub>2</sub>SO<sub>4</sub> and a solar simulator was used as the light source with an irradiation power of 1 W/cm<sup>2</sup>. Figure 1(b) shows schematic of an experimental configuration of the three electrode system. The net acceptor concentration and  $W$  were measured by capacitance-voltage ( $C$ - $V$ ) measurement in the electrolyte at a frequency of 1 kHz and the voltage was scanned from -2 to 0 V vs SCE except for 6H-bulk because of its high resistance characteristics. Spectral responses for p4H, p6H, and p3C were measured in the three electrode system at 0 V vs SCE with light from the solar simulator through a monochromator.

For theoretical photocurrent calculations, we integrated photons absorbed within  $L_D + W$ , and the number of the integrated photons is considered to be converted to photocurrent (photon integral). We also calculated photocurrents using an one dimensional device simulator AMPS-1D, which is based on fundamental equations: Poisson’s equation and the continuity equations for electrons and holes. Using AMPS-1D, we simulated for a solar cell structure with a Schottky barrier with several values of  $\tau$  and  $W$ .<sup>21)</sup> Height of Schottky barriers were fixed at experimental barrier heights obtained from  $C$ - $V$  measurements for p4H,

p6H, and p3C, and a backside ohmic contact was assumed to be located at 300  $\mu\text{m}$  away from the Schottky contact. For such the Schottky barrier cells, even though calculation results do not depend on the surface recombination velocities both for Schottky and ohmic sides, we assumed them as  $10^3$  cm/s which is a similar value to reported one for 4H-SiC.<sup>22,23)</sup> Electron mobilities  $\mu_e$  were set at the reported values ( $1000$ ,  $100$ , and  $1000$   $\text{cm}^2\text{V}^{-1}\text{s}^{-1}$  for 4H-, 6H-, and 3C-SiC, respectively).<sup>24)</sup> To set various  $\tau$  and  $W$ , we changed concentrations of deep recombination centers and an acceptor level.

### 3. Results and discussion

Figure 2 shows the excess carrier decay curves for the 4H-SiC samples measured by the  $\mu$ -PCD method. The decay curve of 4H-bulk shows oscillation from noise because the observed peak size of 4H-bulk is small. The estimated  $\tau$  ranges from 30 to 210 ns, and the bulk sample shows the shortest  $\tau$ . Among the epitaxial 4H-SiC samples, p4H and Less  $N_A$  exhibit almost the same  $\tau$ . The irradiated epitaxial samples show smaller  $\tau$  compared to the as-grown sample and the sample with a higher electron dose show smaller  $\tau$  as reported in ref. 16. Annealing in  $\text{H}_2$  enhanced  $\tau$  of Less  $N_A$  as shown by slow decay in Less  $N_A$   $\text{H}_2$ . We also observed  $\tau$ s for 6H-bulk, p6H, and p3C, and they were  $\sim 50$ ,  $\sim 250$  and  $\sim 90$  ns, respectively.

Figure 3 shows the distribution of net acceptor concentrations for the 4H-SiC samples estimated from  $C$ - $V$  measurements. Among the 4H-SiC samples, 4H-bulk shows the shortest  $W$  and highest net acceptor concentration of  $\sim 2 \times 10^{17}$   $\text{cm}^{-3}$ . For the as-grown epitaxial samples, longer  $W$  and lower net acceptor concentration is attained for Less  $N_A$  than for p4H. The electron irradiation increases  $W$  and decreases the net acceptor concentration with the electron dose. Annealing of Less  $N_A$  in  $\text{H}_2$  ambient increases the net acceptor concentration and slightly decreases  $W$ . We also performed  $C$ - $V$  measurements for p6H and p3C.  $W$  for p6H and p3C were  $\sim 420$  and  $\sim 250$  nm at 0 V vs SCE, respectively, while the net acceptor concentrations for them were  $\sim 1 \times 10^{16}$  and  $\sim 2 \times 10^{16}$   $\text{cm}^{-3}$ , respectively.

Photocurrents observed from the 4H-SiC samples in the three electrode system are shown in Fig. 4. 4H-bulk shows the smallest photocurrent, while Less  $N_A$   $\text{H}_2$  shows the largest photocurrent among the samples. In addition, the currents are almost stable during experiments, which means that the samples are stable against photoelectrochemical corrosion and constantly generate hydrogen.<sup>15)</sup> The photocurrents from the 4H-SiC samples in the two electrode system were also stable during the experiments and had sample

dependence similar to that observed in the three electrode system. We also observed stable photocurrents from the 6H- and 3C-SiC samples in the two and three electrode systems.

From the observed  $\tau$ , we estimated  $L_D = (D_e \cdot \tau)^{0.5}$  by using the diffusion coefficients  $D_e$  estimated from the reported  $\mu_e$  (26, 2.6, and 26 cm<sup>2</sup>/s for 4H-, 6H-, and 3C-SiC, respectively).<sup>24)</sup> We plot the observed photocurrents against sum of the estimated  $L_D$  and observed  $W$  at 0 V vs SCE as shown in Fig. 5 for the 4H-SiC samples. The observed photocurrents by the two and three electrode systems monotonically depend on  $L_D + W$ . In this figure, we also show the line calculated by photon integral and plots from calculations by AMPS-1D with several  $\tau$  and  $W$ . These calculations also show a monotonical dependence of photocurrents on  $L_D + W$ . In addition, the observed photocurrents are not so small compared with the calculations; for example, the photocurrent from Less  $N_A$  is ~50% of photon integral.

For the 6H-SiC samples, the observed photocurrents are shown against  $L_D + W$  in Fig. 6. Calculations are also shown as in this figure. Although we show plots only from two samples for the observed photocurrents, the photocurrents increase with  $L_D + W$  as in the calculations. Compared with calculated photocurrent by photon integral, the observed photocurrent for p6H is ~45%.

We only employed one 3C-SiC sample in this study, and we also plot the observed photocurrent against  $L_D + W$  along with calculations in Fig. 7. The calculations show dependence on  $L_D + W$  the same as for 4H- and 6H-SiC. Compared with the calculations, the observed photocurrent is only ~8%.

The photocurrent depends on  $L_D + W$  as revealed for the 4H- and 6H-SiC samples. Thus, to enhance the conversion efficiency, increase of  $L_D$  and  $W$  will be effective. In contrast to the 4H- and 6H-SiC samples, the 3C-SiC sample exhibited photocurrent much smaller than the calculated one. To confirm effective  $L_D$  (equivalent to effective  $\tau$ ) and  $W$ , we measured spectral responses from an epilayer for each polytype, p4H, p6H and p3C.

Figure 8 shows a spectral response for p4H and p6H. The lines show calculated responses by the photon integral and AMPS-1D with  $W$  of 0.4  $\mu\text{m}$  and  $\tau = 100$  ns which is a similar value to those obtained by  $\mu$ -PCD. For wavelengths below 270 nm, the light power is so small that the efficiency cannot be measured correctly. The experimental efficiency for p6H is higher than that for p4H as expected from their bandgap and photocurrents in Figs. 5 and 6. Compared with calculations, the experimental efficiencies are small, but the responses at the longer wavelength side are not significantly different between the experiment and the calculations. Therefore, effective  $\tau$  for p4H and p6H would be similar to  $\tau$  obtained by  $\mu$ -PCD, 150-250 ns.

Figure 9 shows a spectral response for p3C, and we also show calculations with  $W$  of 0.3  $\mu\text{m}$  and  $\tau = 10$  and 100 ns. The experimental response has a shape completely different from the calculated ones and is significantly smaller in the longer wavelength side. Therefore, effective  $\tau$  for p3C is smaller than 10 ns, which is much smaller than  $\tau$  obtained by  $\mu$ -PCD, 90 ns. This result suggests that p3C has structural defects decreasing effective  $\tau$  and reducing responses in the longer wavelength side. In fact, p3C was grown on a 6H-SiC substrate and thus was heteropolytypic epitaxially grown. On the other hand, the 4H- and 6H-SiC epitaxial samples were grown under homopolytype conditions. The homopolytypic growth was performed on off-axis substrates and proceeded by the step flow mechanism resulting in dislocation densities similar to those in the substrates.<sup>25)</sup> In contrast, heteropolytypic growth was performed on an on-axis substrate, and the crystal was grown by two-dimensional island formation and subsequent spiral growth of the island.<sup>26)</sup> After the growth, threading dislocations are formed between the grown islands and the density of dislocations should be high compared with the substrate. Such dislocations will act as trapping and/or recombination centers of electrons.<sup>27-29)</sup> Therefore, we consider that heteropolytypic grown p3C has a large number of dislocations, i.e., structural defects, reducing effective  $\tau$  in the epilayer. Improvement of the 3C-SiC growth technique will increase effective  $\tau$  and the solar-to-hydrogen conversion efficiency by 3C-SiC photocathodes.

#### 4. Conclusions

We observed  $\tau$  and  $W$  in 4H-, 6H-, and 3C-SiC samples and estimated sum of  $L_D$  and  $W$  by using reported  $D_e$ . We also observed photocurrents from photocathodes using the samples. By comparison of  $L_D + W$  with the photocurrents, we found monotonical dependence of photocurrents on  $L_D + W$  for the 4H- and 6H-SiC photocathodes, and this dependence agrees with the calculated photocurrents. On the contrary, the 3C-SiC photocathode shows much smaller photocurrents compared with calculations. From the spectral responses of the photocathodes, we found that 3C-SiC has smaller effective  $\tau$  than that measured by  $\mu$ -PCD. These results suggest that enhancement of  $\tau$  and  $W$  is effective for improvement of conversion efficiencies for 4H- and 6H-SiC. To improve the efficiency from 3C-SiC, decrease of structural defects reducing effective  $\tau$  is required, and thus development of growth techniques of 3C-SiC is very important for realization of hydrogen generation by 3C-SiC photocathodes.

## **Acknowledgments**

The authors thank Mr. T. Okuda, Professor J. Suda and Professor T. Kimoto for hydrogen treatment. This work is supported by a Grant-in-Aid for Scientific Research on Innovative Areas "Artificial photosynthesis (AnApple)" 25107516, the Takahashi Industrial and Economic Research Foundation, and the Tatematsu Foundation.

## References

- 1) W. Grochala and P.P. Edwards, *Chem. Rev.* **104**, 1283 (2004).
- 2) I. Akkermana, M. Janssenb, J. Rochac, and R.H. Wijffels, *Int. J. Hydrogen Energy* **27**, 1195 (2002).
- 3) K. Maeda and K. Domen, *J. Phys. Chem. Lett.* **1**, 2655 (2010).
- 4) A.J. Bard and M.A. Fox, *Acc. Chem. Res.* **28**, 141 (1995).
- 5) D.A. Tryk, A. Fujishima, and K. Honda, *Electrochim. Acta* **45**, 2363 (2000).
- 6) O. Khaselev and J. A. Turner, *Science* **280**, 425 (1998).
- 7) J.A. Turner, *Science* **305**, 972 (2004).
- 8) T. Bak, J. Nowotny, M. Rekas, and C.C. Sorrell, *Int. J. Hydrogen Energy* **27**, 991 (2002).
- 9) S.U.M. Khan, M. Al-Shahry, and W.B. Ingler, *Science* **297**, 2243 (2002).
- 10) S.U.M. Khan, and J. Akikusa, *J. Electrochem. Soc.* **145**, 89 (1998).
- 11) A.W. Mau, C. Huang, N. Kakuta, A.J. Bard, A. Campion, M.A. Fox, J.M. White, and S.E. Webber, *J. Am. Chem. Soc.* **106**, 6537 (1984).
- 12) T. Yasuda, M. Kato, M. Ichimura, and T. Hatayama, *Appl. Phys. Lett.* **101**, 53902 (2012).
- 13) T. Yasuda, M. Kato, M. Ichimura, and, T. Hatayama, *Mater. Sci. Forum* **740-742**, 859 (2013).
- 14) T. Yasuda, M. Kato, and M. Ichimura, *Mater. Sci. Forum* **717-720**, 585 (2012).
- 15) M. Kato, T. Yasuda, and K. Miyake, *Int. J. Hydrogen Energy* **39**, 4845 (2014).
- 16) K. Miyake, T. Yasuda, M. Kato, M. Ichimura, T. Hatayama, and T. Ohshima, *Mater. Sci. Forum* **778-780**, 503 (2014).
- 17) M. Kato, Y. Matsushita, M. Ichimura, T. Hatayama, and T. Ohshima, *Jpn. J. Appl. Phys.* **51**, 028006 (2012).
- 18) M. Kato, K. Yoshihara, M. Ichimura, T. Hatayama, and T. Ohshima, *Jpn. J. Appl. Phys.* **53**, 04EP09 (2014).
- 19) T. Okuda, T. Kimoto, and J. Suda, *Appl. Phys. Express* **6**, 121301 (2013).
- 20) T. Okuda, T. Miyazawa, H. Tsuchida, T. Kimoto, and J. Suda, *Appl. Phys. Express* **7**, 085501 (2014).
- 21) <http://www.ampsmodeling.org/>
- 22) M. Kato, A. Yoshida, and M. Ichimura, *Jpn. J. Appl. Phys.* **51**, (2012).
- 23) Y. Mori, M. Kato, and M. Ichimura, *J. Phys. D* **47**, 335102 (2014).
- 24) O. Madelung ed. *Data in Science and Technology, Semiconductors Group IV Elements and III-V Compounds* (Springer, Berlin 1991).
- 25) T. Kimoto, A. Itoh, and H. Matsunami, *Phys. Status Solidi B* **202**, 247 (1997).

- 26) Z.Y. Xie, J.H. Edgar, B.K. Burkland, J.T. George, and J. Chaudhuri, *J. Cryst. Growth* **224**, 235 (2001).
- 27) G. Feng, J. Suda, and T. Kimoto, *Jpn. J. Appl. Phys.* **49**, 090201 (2010).
- 28) M. Ichimura, H. Tajiri, Y. Morita, N. Yamada, and A. Usami, *Appl. Phys. Lett.* **70**, 1745 (1997).
- 29) M. Ichimura, N. Yamada, H. Tajiri, and E. Arai, *J. Appl. Phys.* **84**, 2727 (1998).

## Figure Captions

**Fig. 1.** (Color online) Schematics of (a) the sample placed on a plastic plate, and (b) experimental configuration of the three electrode system.

**Fig. 2.** (Color online) Excess carrier decay curves for the 4H-SiC samples.

**Fig. 3.** (Color online) Distributions of the net acceptor concentration for the 4H-SiC samples.

**Fig. 4.** (Color online) Photocurrents observed from the photocathodes by the 4H-SiC samples.

**Fig. 5.** (Color online) Dependence of photocurrent on the sum of  $L_D + W$  for the 4H-SiC samples. The closed symbols are experimental results. The line and open symbols are calculated by photon integral and AMPS-1D with various  $\tau$  and  $W$ , respectively (values of  $W$  are indicated in the legend).

**Fig. 6.** (Color online) Dependence of photocurrent on the sum of  $L_D + W$  for the 6H-SiC samples.

**Fig. 7.** (Color online) Dependence of photocurrent on the sum of  $L_D + W$  for the 3C-SiC samples.

**Fig. 8.** (Color online) Spectral responses for the 4H- and 6H-SiC photocathodes. The plots are experimental results, while the lines are calculated by photon integral and AMPS-1D with  $\tau = 100$  ns, respectively.

**Fig. 9.** (Color online) Spectral response for the 3C-SiC photocathode. The plots are experimental results, while the lines are calculated by photon integral and AMPS-1D with  $\tau$  of 10 and 100 ns.

**Table I.** Thickness and substrate of the samples.

| Polytype | Sample                        | Thickness<br>( $\mu\text{m}$ ) | Substrate                          |
|----------|-------------------------------|--------------------------------|------------------------------------|
|          | 4H-bulk                       | 350                            | —                                  |
| 4H-SiC   | Less $N_A$ and Less $N_A H_2$ | 10                             | (0001) $4^\circ$ off-axis 4H-SiC   |
|          | p4H, ele16 and ele17          | 10                             | (0001) $8^\circ$ off-axis 4H-SiC   |
|          | 6H-bulk                       | 400                            | —                                  |
| 6H-SiC   | p6H                           | 20                             | (0001) $3.5^\circ$ off-axis 6H-SiC |
| 3C-SiC   | p3C                           | 20                             | (0001) on-axis 6H-SiC              |

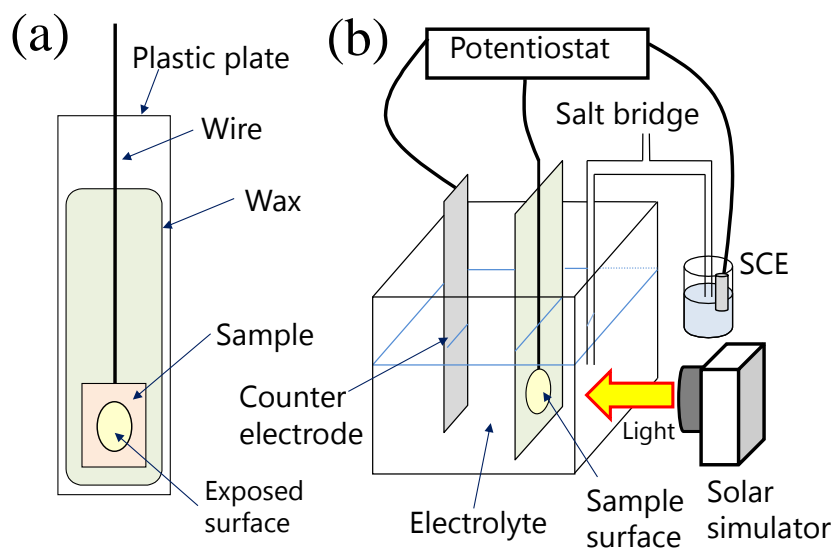


Fig.1. (Color Online)

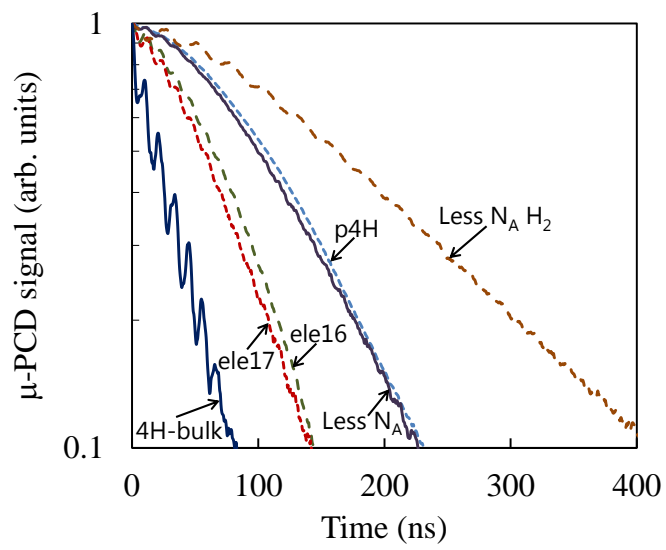


Fig.2. (Color Online)

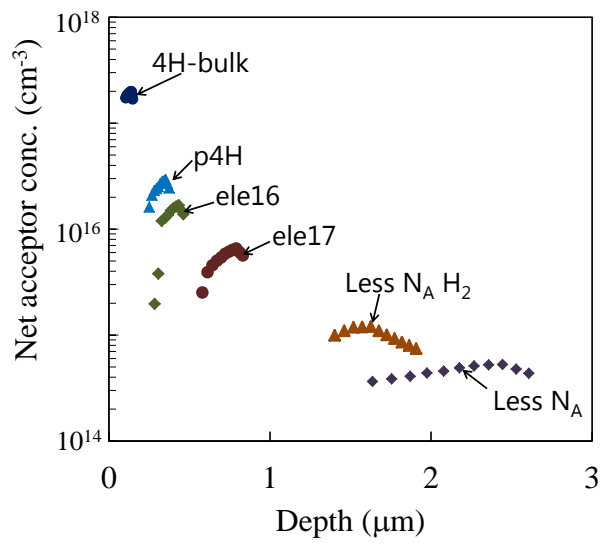


Fig. 3. (Color Online)

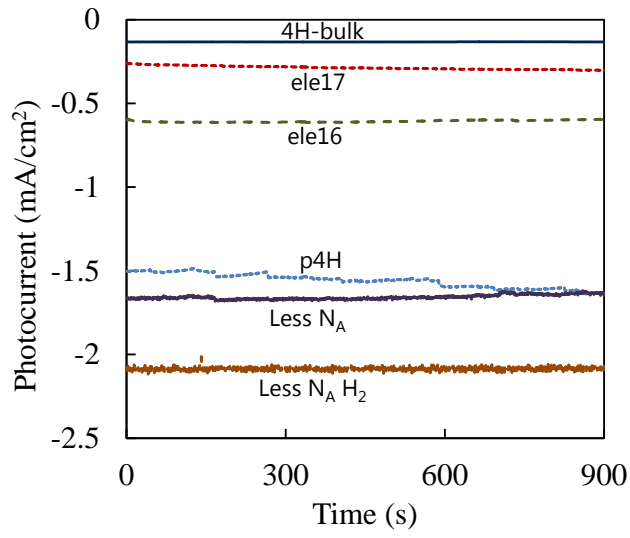


Fig. 4. (Color Online)

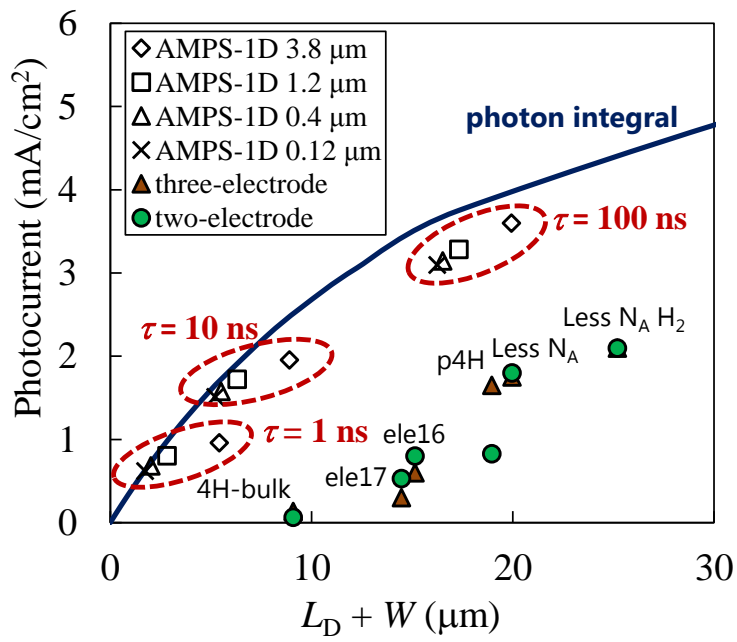


Fig. 5. (Color Online)

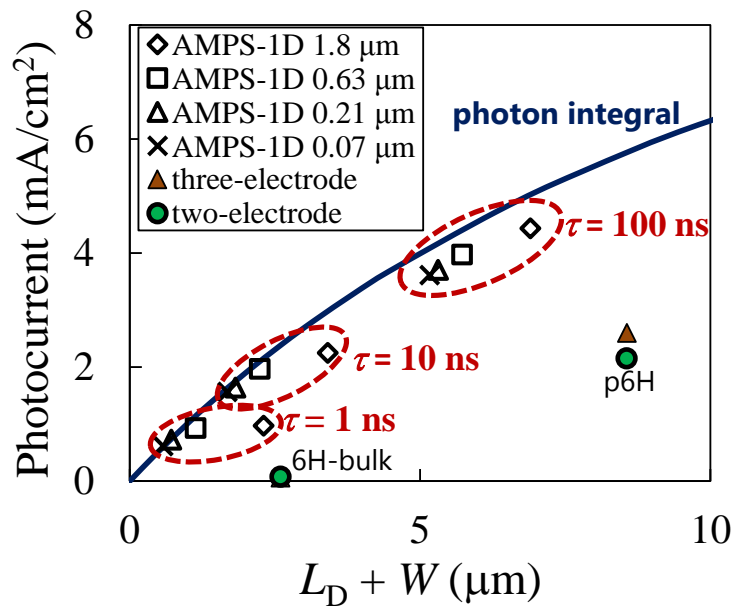


Fig. 6. (Color Online)

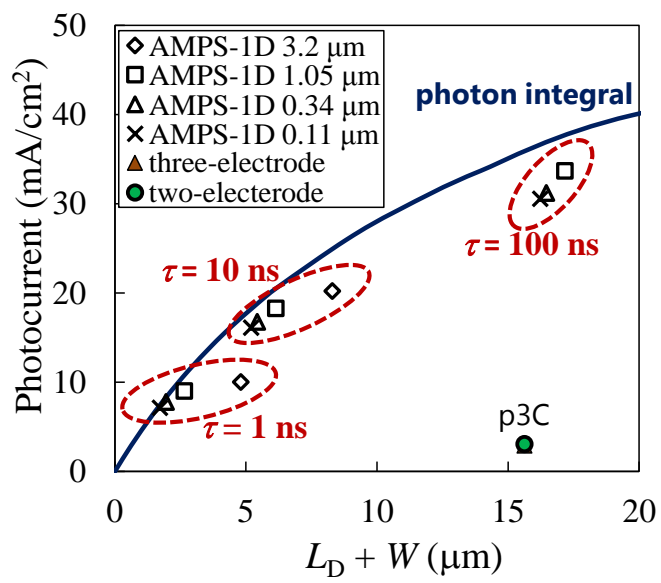


Fig. 7. (Color Online)

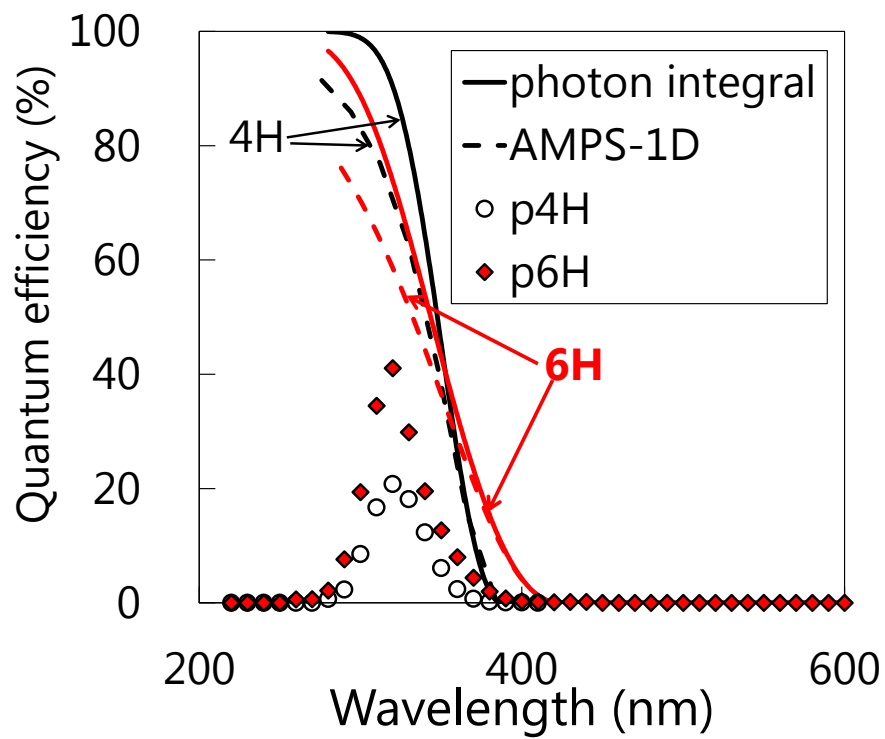


Fig. 8. (Color Online)

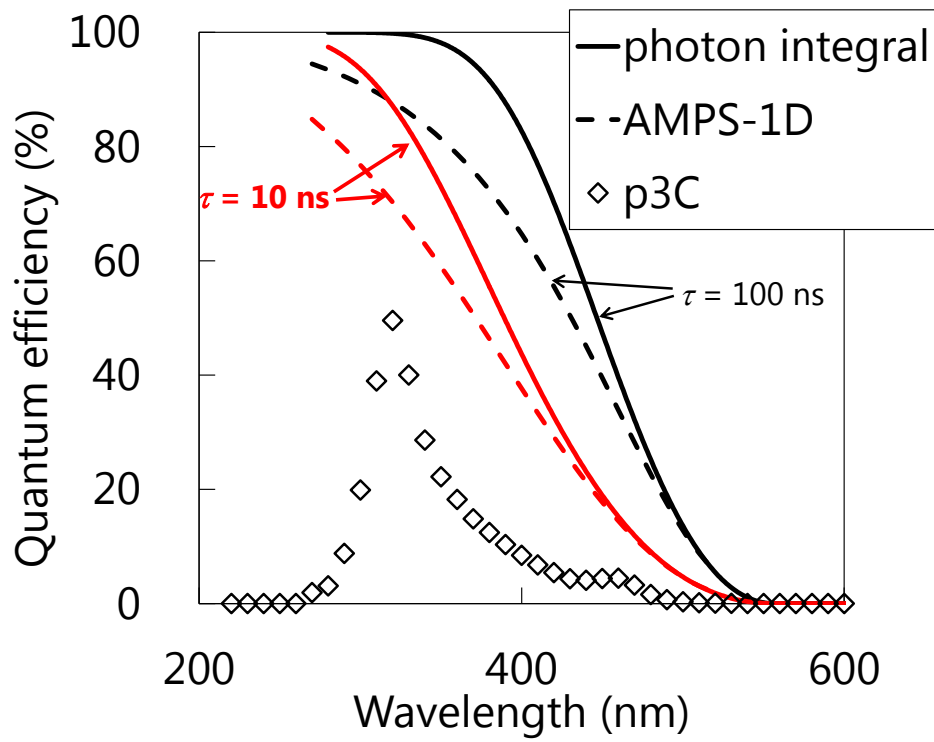


Fig. 9. (Color Online)